

Title: A Personalized Fluid-structure Interaction Modeling Paradigm for Aorta in Human Fetuses

Ya Tang^{1,*}, MS; Guihong Chen^{2,*}, MD; Liquan Sun³, MD PhD; Lisa Hornberger⁴, MD; Zhenglun Alan Wei¹, PhD; Shuping Ge⁵, MD

¹Department of Biomedical Engineering, University of Massachusetts Lowell, Lowell, MA, USA

²Medical Ultrasound Department, The Fourth Hospital of Shijiazhuang, Shijiazhuang, China

³Division of Cardiology, Department of Pediatrics, The Hospital for Sick Children, University of Toronto, Toronto, Canada

⁴Fetal & Neonatal Cardiology Program, University of Alberta, Edmonton, Canada

⁵Department of Pediatric and Adult Congenital Cardiology, Geisinger Heart and Vascular Institute, Geisinger Clinic

* These authors contributed equally to the current work

Please send the correspondence of the current work to

Name: Zhenglun Alan Wei, PhD

Address: Falmouth Hall 302, One University Ave, Lowell, MA, 01854

Phone: 978-934-3754

Fax:

E-mail: ZhenglunAlan_Wei@uml.edu

Name: Shuping Ge, MD, FACC, FAHA, FASE

Address: 100 N. Academy Avenue, Danville, PA 17822

Phone: 570-271-6466

Fax: 570-214-1480

E-mail: sge@geisinger.edu

Word Count: 3298 (Limit: 3500)

Keywords

Personalized cardiovascular simulation, medical image processing, the fetal circulation

Abstract (Word Count: 329; Limit: 350)

Background

Congenital heart disease (CHD) is the most common birth defect and a leading cause of death and chronic illness in newborns, infants, and children. Prenatal screening and identification of CHD are critically important, but their availability and accuracy are limited by current fetal imaging techniques. To date, few models have been developed for fetal circulation. Considering the fetal aorta is frequently affected in CHDs, this study aims to develop and validate a novel model to assess the hemodynamics of the fetal aorta.

Methods

Fetal echocardiography (FE) and Doppler were used to build a fluid-structure interaction (FSI) model that assesses the fetal aorta in 3 dimensions. An inverse approach was used to obtain the material property. An iterative method was also proposed to estimate the outflow boundaries. The FSI results have been validated against clinically measured dimensions and velocities over a cardiac cycle for aortas in 4 healthy fetuses.

Results

The proposed FSI model has been implemented in 4 healthy fetal aortas representing a range of gestational age (GA = 23.5-36.0 weeks). The iterative method successfully estimated Windkessel parameters that match *in vivo* measured flow rates at outflow boundaries. The FSI model has been validated using *in vivo* velocity waveforms at the aortic isthmus. The resultant L_2 -norm was [12.5%, 16.4%], which is acceptable based on previous simulation studies. Also, the aortic stiffness of the fetal aorta decreased with GA, adding evidence to an existing controversy about the trend between aortic stiffness and GA.

Conclusions

This study represents the first-of-its-kind endeavor of a rigorously validated personalized flow model for fetal circulation. The developed FSI model has been successfully validated for four subjects. The model was also used to obtain new evidence of fetal aortic development and growth.

A. Introduction

Congenital heart disease (CHD) is the most common birth defect and a leading cause of death and chronic disease in newborns, infants, and children [1-3]. Prenatal screening and identification of CHD provide the earliest window of opportunity to improve the understanding of pathogenesis, timely diagnosis/prognosis, parental counseling, safety, and effective therapy for optimal perinatal and long-term outcomes [4, 5]. However, there are many challenges in clinical care and innovation in CHD due to the lack of animal models, rarity, and limited resolutions of contemporary fetal imaging methodology for accurate diagnosis and prognosis of CHD before birth [6, 7].

Computational flow modeling has been used to augment medical imaging modalities and capture high-fidelity hemodynamics in the cardiovascular system in a personalized fashion. Many previous studies have used computational models to understand and uncover the mechanism, improve diagnosis/prognosis, and develop treatment methods such as medical devices and therapies for adult and pediatric heart diseases [8-11]. However, data for developing a computational model for fetal circulation is scarce. Fewer have been rigorously validated against clinical measurements. Wiputra et al. developed a computational model to simulate the fetal right ventricle and obtained "generally good agreements" between their simulated data and a range of published data [12]. Later, the same group presented a plausible study to validate their model against clinically measured velocity by echocardiography. However, their validation focused on the velocity at specific time points of a cardiac cycle, e.g., at peak systole, instead of time-resolved quantities over the whole cardiac cycle [13]. Last year, Salman et al. employed the model from Wiputra's study and confirmed that the model produces results qualitatively agreed with the literature data [14].

The fetal aorta is involved in many CHDs, for example, coarctation of the aorta, patent ductus arteriosus, and transposition of the great arteries. Many computational models have been developed for the aorta in pediatric or adult patients [15-20]. However, the fetal aorta is NOT a smaller version of the pediatric or adult ones, which has an additional vessel (the ductus arteriosus, Fig. 1) that makes the anatomy and flow conditions more complex.

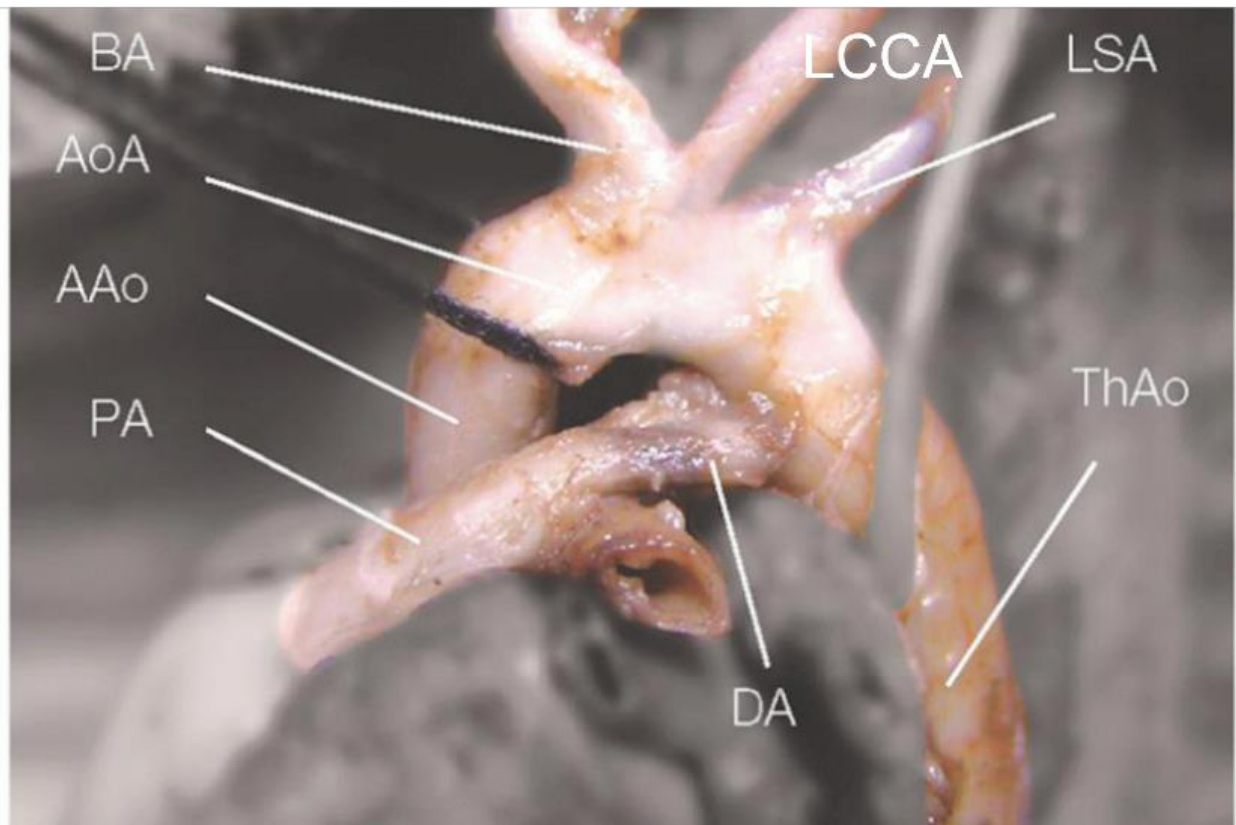


Figure 1 A illustration of the fetal aorta in a healthy individual [21]. AAo: ascending aorta, AoA: aortic arch, BA: brachiocephalic artery, DA: ductus arteriosus, LCCA: left common carotid artery, LSA: left subclavian artery, PA: pulmonary artery, and ThAo: thoracic aorta,

Previous studies used zero-dimensional lumped parameter models that simulate the hemodynamics in the fetal aorta using simplified relation between flow rate and pressure drop [22-25]. Recent studies used computational fluid dynamics models to capture high-fidelity three-dimensional hemodynamics for the fetal aorta [26-28]. However, these models overlook many important patient characteristics, e.g., the material properties of the vessel. This could lead to significant errors in calculating hemodynamic metrics [15, 19, 20, 29]. More importantly, none of these models have been validated. Therefore, to date, there is no rigorously validated computational model for the fetal aorta.

Thus, the objective of this study is to develop a novel, personalized flow model to assess the hemodynamics of the fetal aorta and validate this model using *in vivo* measurements. The developed model will involve personalized anatomy, flow, and material property of the fetal aorta. The validated model can be used to understand the pathogenesis of CHD related to the fetal aorta, improve pertinent

diagnostic/prognostic methods, and investigate the feasibility, safety, and efficacy of therapeutic strategies.

B. Materials and Methods

B.1 Study Subjects

The patients included in this study were retrospectively selected with the following criteria:

- **Inclusion Criteria:** 1) Singleton pregnancy; 2) gestational age (GA) > 20 weeks and < 40 weeks; 3) no structural defect, heart failure, or arrhythmia in the fetus.
- **Exclusion Criteria:** (1) Cardiac condition (e.g., fetal cardiac dysfunction and/or fetal hydrops, fetal arrhythmia, abnormal baseline heart rate [<110 bpm or > 160 bpm]); (3) multiple pregnancies, and (2) fetal growth restriction (<3 rd centile).

Standard ultrasound systems (GE Voluson E-10) were used to acquire 2D, 3D, and Doppler fetal echocardiography (FE): the long-axis acquisition should capture the center plane of the aortic arch with the ascending aorta (AAo), aortic arch, the descending aorta (DAo), the brachiocephalic artery (BA), the left common carotid artery (LCCA), and the left subclavian artery (LSA). The short-axis acquisition should exhibit the center plane of the 3-vessel view, including the aortic and ductal arch structures. 2D FE images were also acquired. Doppler velocity tracing was recorded for ascending aorta (AAo), ductus arteriosus (DA), aortic isthmus (AoI), and DAo. There was no clinical measurement in the left common carotid artery (LCCA), left subclavian artery (LSA), and brachiocephalic artery (BA), primarily because of small vessel sizes and challenges in an appropriate field of view.

B.2 Anatomy Reconstruction

3D FE acquisition usually has ~30 slices spatially (with 0.5 mm thickness) and 7-13 time frames. The frame of the smallest volume of the fetal aorta (during end-diastole) was chosen for anatomical reconstruction using SimVascular [30].

Firstly, the center plane of the fetal aorta was identified (Fig. 2b), highlighting the center plane of the aortic arch, as well as its bifurcations to the LCCA, LSA, and BA. The next step was identifying the bifurcation between the aortic arch and DA. After the centerline of the aortic arch, the LCCA, LSA, BA,

and DA were identified and then lofted, assuming their structure to be circular cylinders (Fig. 2c). The diameter of the lofted vessels was compared with the clinical measurements done in 2D FE, which is the current gold standard. All 2D FE measurements were verified by SG (the last author), who has more than 20 years of clinical experience in acquiring and analyzing FE images and data.

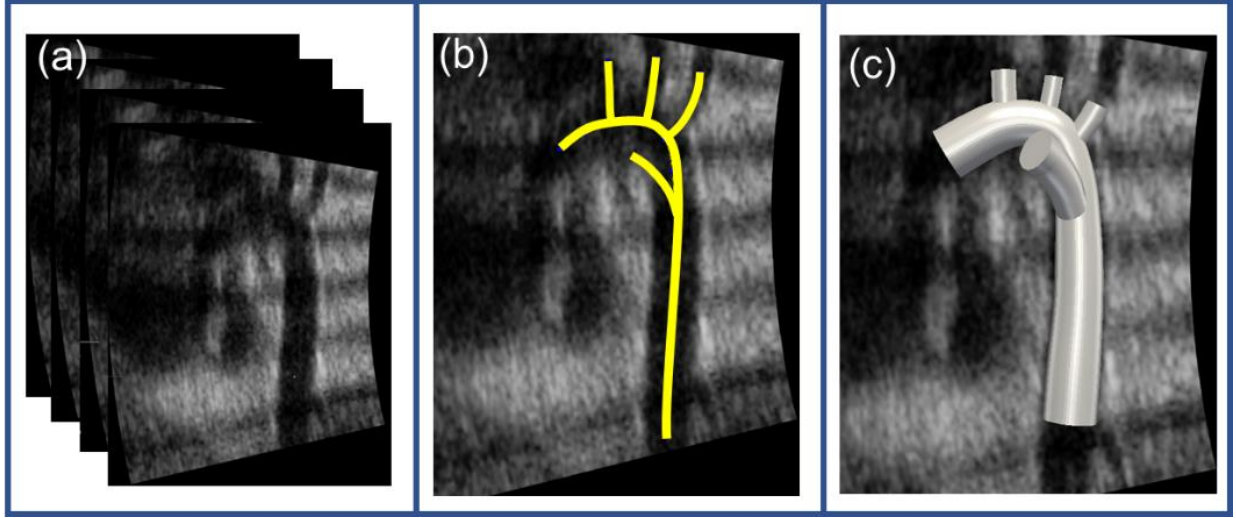


Figure 2 Workflow of anatomical reconstruction: (a) a schematic drawing of a stack of DICOM images from 3D FE acquisition, (b) highlighting the center line of all vessels, and (c) a sample of reconstructed anatomy

B.3 Flow Segmentation

Doppler data were segmented using PlotDigitizer (a free web-based tool), Fig. 3a. The ultrasound machine implemented an angle correction (α in Fig. 3b) on the velocity tracking. However, this angle may have presented a discrepancy when compared to the angle between the ultrasound beam and the true centerline of the vessel (β in Fig. 3b). If the discrepancy ($\beta - \alpha$) was larger than 20 degrees, a further angle correction was implemented on the velocity waveforms:

$$V_{corrected} = \frac{\cos \alpha}{\cos \beta} V_{segmented} \quad (1)$$

The vessel flow rate (Q) was then calculated using the vessel diameter and corrected velocity.

$$Q = \left(\pi D^2 V_{corrected} \right) / 4 \quad (2)$$

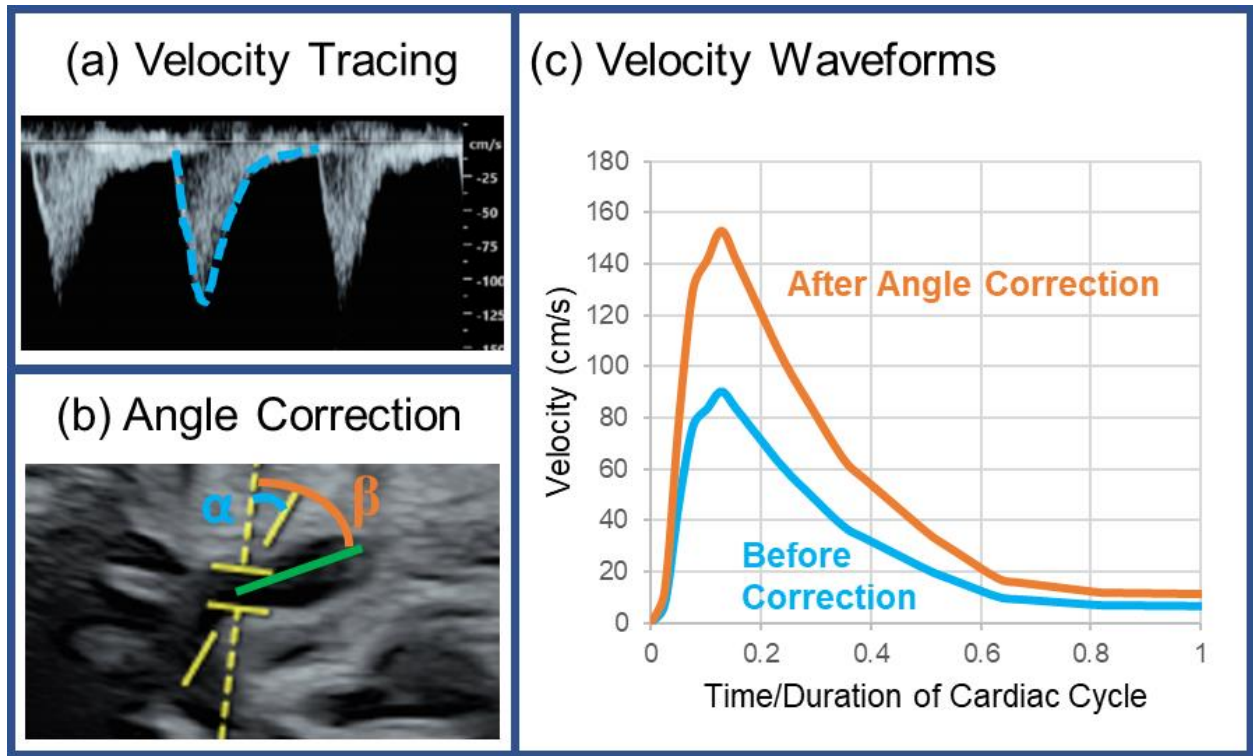


Figure 3 Workflow of flow segmentation

B.4 The Estimation of Material Property

The material property of a fetal aorta was estimated using an in-house inverse method with a finite element analysis (FEA) [31]. The process started with a random guess of Young's modulus. A pulse pressure (ΔP) was applied inside the reconstructed fetal aorta (at its smallest volume). The FEA outputted a deformed fetal aorta based on the current value of Young's modulus. The vessel diameters in the deformed state were compared against clinical measurements from FE. If the discrepancies were found to have exceeded 5%, Young's modulus was adjusted and used to perform another FEA.

Since the invasive measure of ΔP was not available, we adopted the previously published values dependent on the GA [25, 32], referring to ΔP_{GA} .

$$\Delta P_{GA} (mmHg) = 0.39 \times GA + 13.44 \quad (3)$$

Also, the FEA used three assumptions commonly accepted by previous studies: (1) a homogenous, linear elastic material model [19, 33], (2) the vessel wall thickness as 15% of the diameter [25, 34], and (3) the Poisson ratio as 0.499 [32-34].

B.5 Boundary Conditions & Windkessel Model

The in-house user-defined function was used to apply Womersley velocity profiles to the AAO and DA [35, 36] along with imposing 3-element Windkessel models on BA, LCCA, and LSA, and DAo, as shown in Fig. 4.

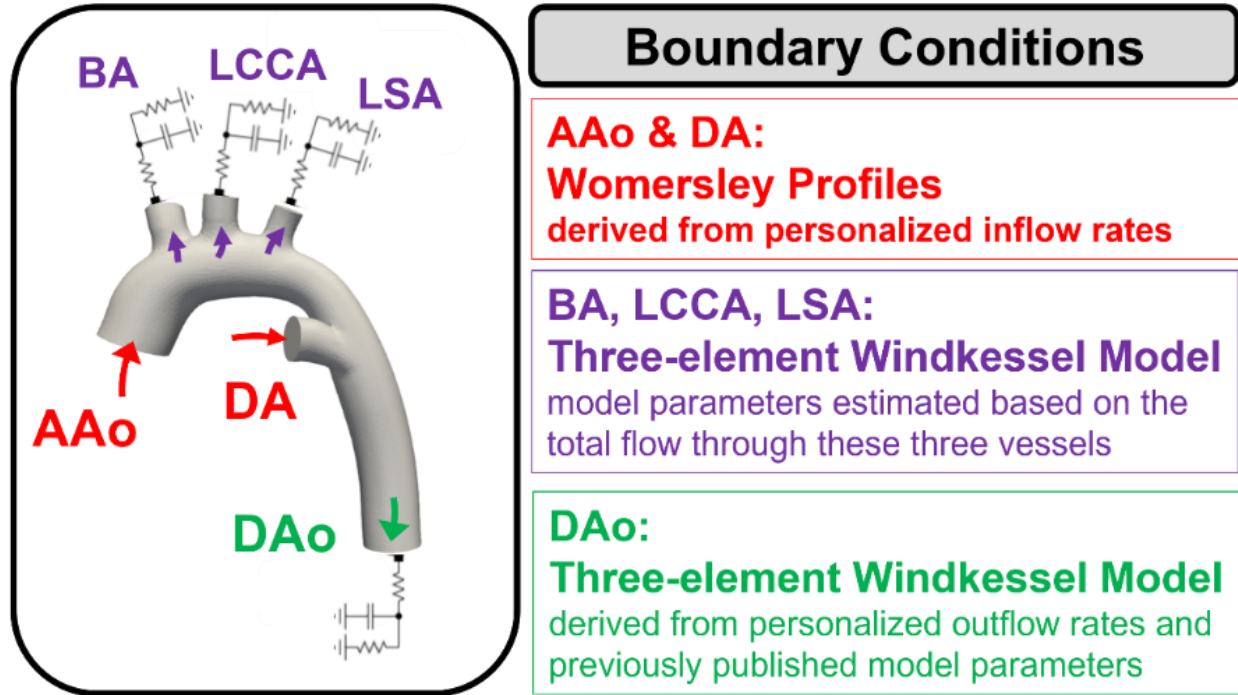


Figure 4 Boundary conditions of the computational model.

The estimation of Windkessel parameters consists of two parts:

1. Without *in vivo* flow measurements for BA, LCCA, and LSA, the parameters for these three branches were estimated using their total flow rate: $Q_{3\text{branches}} = Q_{\text{AAo}} + Q_{\text{DA}} - Q_{\text{DAo}}$. A 3-element Windkessel model was built based on $Q_{3\text{branches}}$ and ΔP_{GA} . The parameters from this model (based on $Q_{3\text{branches}}$) were then "split" to the BA, LCCA, and LSA based on their respective vessel diameters [16]. It is worth noting that ΔP_{GA} from the literature derived for DAo [25, 32]; but there is a pressure drop from AAo (and the three branches) to DAo. Therefore, we used ΔP_{GA} here as a better initialization value than a random one. Step 3 was for remedying this pressure drop.
2. Once the model parameters of BA, LCCA, and LSA were determined, FSI was run, adjusting the model parameters for DAo till the Q_{DAo} from FSI matched the *in vivo* measured value. At this point, the FSI-derived ΔP of DAo was lower/higher than that of AAo (and the three branches), which

was set as ΔP_{GA} in Step 1. Ultimately, the objective was to match the FSI-derived ΔP of DAo to ΔP_{GA} as the latter value was for DAo [25, 32].

3. Primarily driving the pulse pressure in the 3-element Windkessel model, the proximal resistance of all vessels (DAo and the three branches) were simultaneously scaled up/down till the FSI-derived ΔP of DAo matches the ΔP_{GA} .

B.6 Fluid-structure Interaction Modeling

The fluid and solid domains were meshed separately using the ANSYS meshing module. The solid shell was first discretized using the triangles method. Then, the fluid domain was meshed with tetrahedral cells. Transient FSI simulations were conducted using ANSYS System Coupling. The fluid and structural models interacted in a partitioned approach. The fluid domain was dynamically re-meshed during the computation, and the diffusion-based smoothing algorithm was applied to maintain the mesh quality. The quasi-Newton stabilization method was used to address coupling instability and improve convergence. No turbulence modeling was involved because the Reynolds numbers based on AAo for the subjects were 417 ± 78 . Blood was treated as single-phase, non-Newtonian fluids using the previously published relation for fetal aortas [25].

$$\mu = \frac{(1.15 + 0.075 * GA)}{1000} \text{ (kg/m-s)} \quad (4)$$

The primary outputs of the FSI model were velocity and wall shear stress (WSS). The normalized L_2 error norm of the flow quantity φ was calculated by the following equations:

$$L^2\text{-norm} = \sqrt{\int \left[\varphi_{FSI}(t) - \varphi_{echo}(t) \right]^2 dt} \quad (5)$$

$$\varphi(t) = \varphi(t) / \left(\overline{\varphi_{echo}} \right) \quad (6)$$

where $\overline{\varphi_{echo}}$ is the time-averaged value of the quantity.

C. Results

C.1 Patient Selection

The personalized anatomy for all subjects has been successfully reconstructed, as shown in Fig. 5. All anatomies were plotted in the same dimensional scale to facilitate the visualization of their size differences.

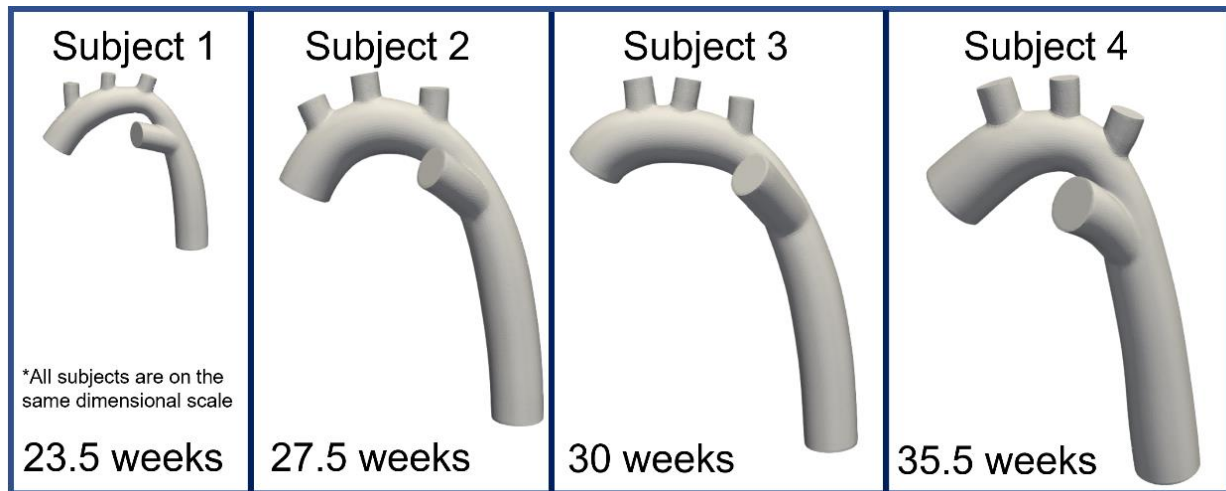


Figure 5 Personalized anatomies for all subjects with the corresponding gestational age.

These individuals cover the typical GA range that was feasible for FE acquisition. In Fig. 6, the vessel size determined by 2D FE and FSI was also compared. Good agreements were obtained, with the value from 2D FE for each vessel falling between the highest and lowest values from FSI.

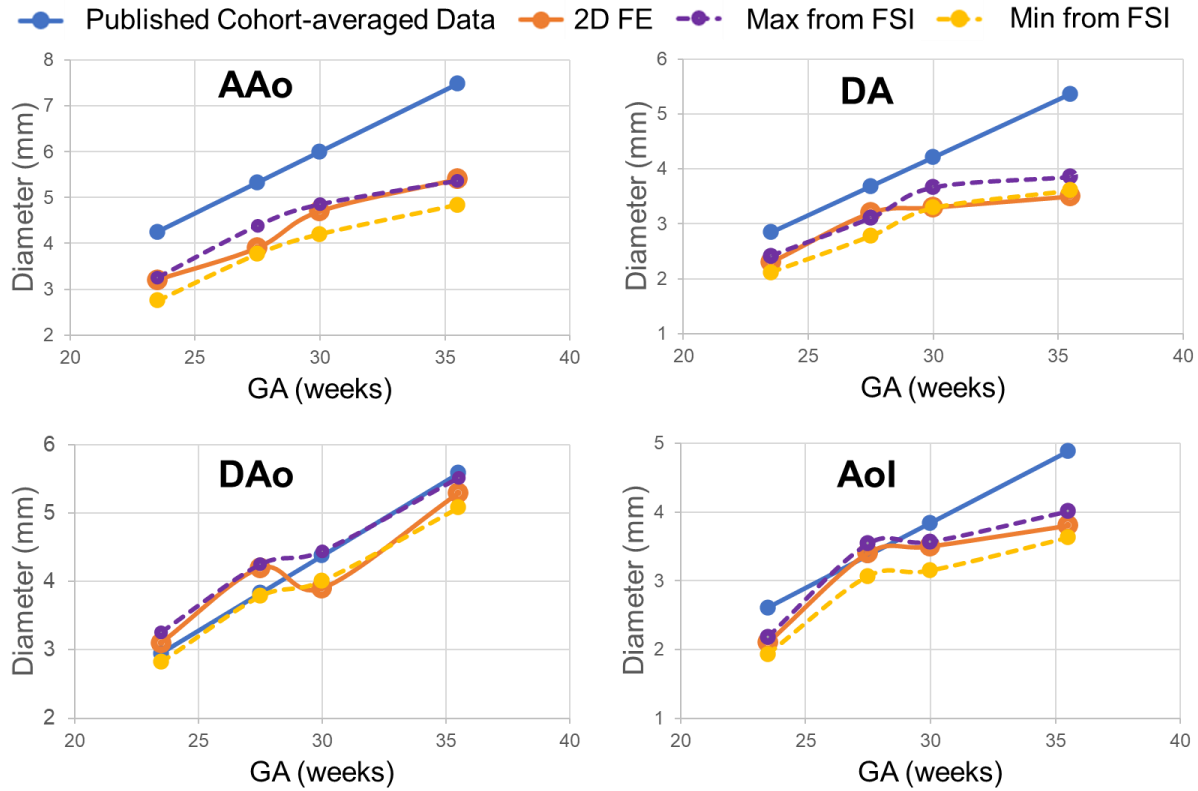


Figure 6 Comparisons of vessel sizes between 2D FE, FSI, and published cohort-averaged data [25]

Table 1 tabulates the flow rate of AAO, DA, and DAo. All vessels presented an increasing flow rate with GA.

Table 1 Summary of flow rate for ascending aorta (AAo), ductus arteriosus (DA), and descending aorta (DAo).

| Flow Rate (mL/min) | AAO | DA | DAO |
|------------------------|-------|-------|-------|
| Subject 1 (23.5 weeks) | 131.7 | 56.3 | 110.3 |
| Subject 2 (27.5 weeks) | 238.1 | 175.9 | 338.4 |
| Subject 3 (30 weeks) | 333.2 | 213.9 | 440.9 |
| Subject 4 (35.5 weeks) | 587.5 | 194.9 | 590.5 |

C.2 Mesh-independence Study

The mesh-independence study was conducted based on subject 4. The study started with a $D_{avg}/12.5$ edge size, where D_{avg} is the average diameter of inflow boundaries, i.e., DAo and DA. Every refinement reduced the edge size by 20%, resulting in a ~50% reduction in mesh cell volume.

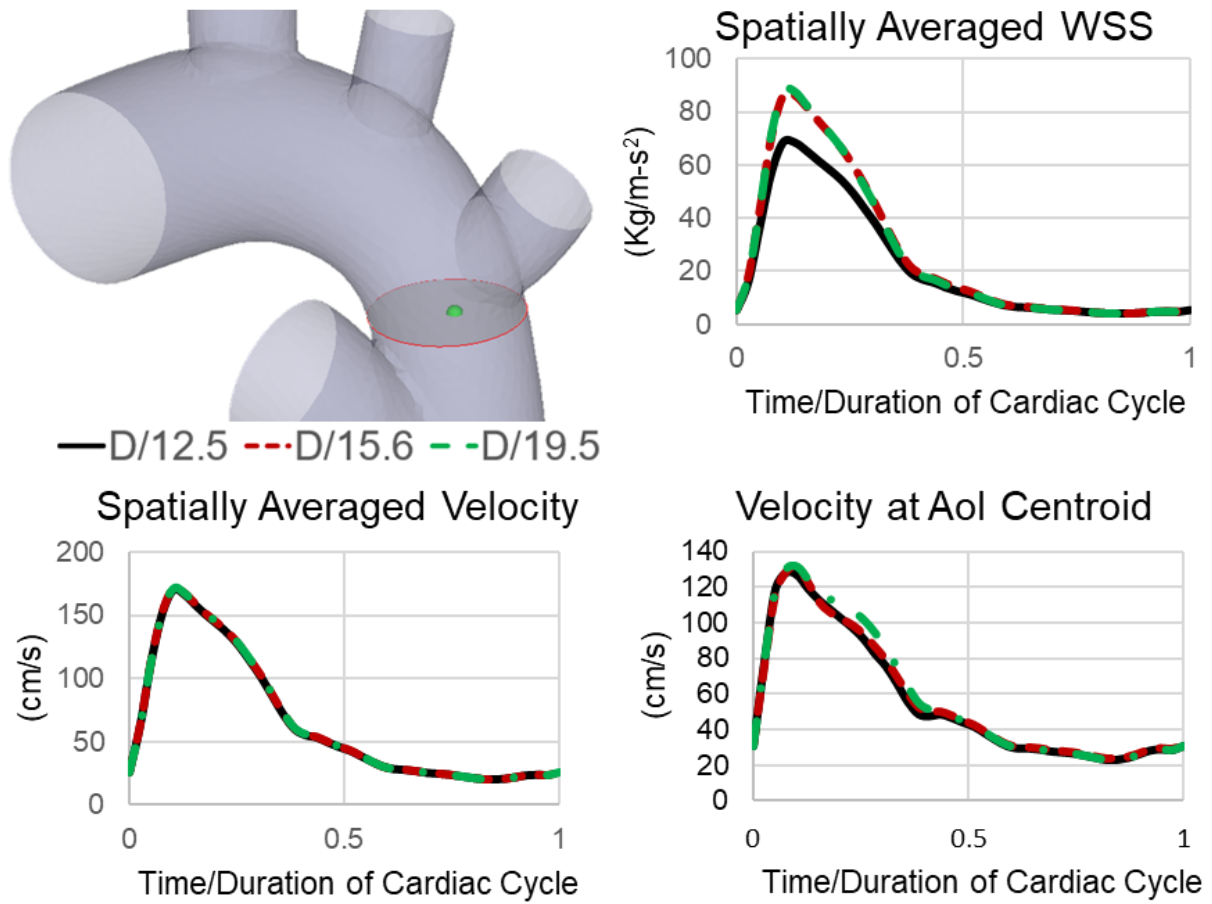


Figure 7 Results of mesh independence study for a representative subject.

Figure 7 exemplifies that the $D_{avg}/15.6$ produced mesh-independent values (less than 3% changes [35, 37]). Therefore, this mesh was chosen for all simulations, resulting in around 0.25 million tetrahedral cells per mesh.

C.3 Material Properties

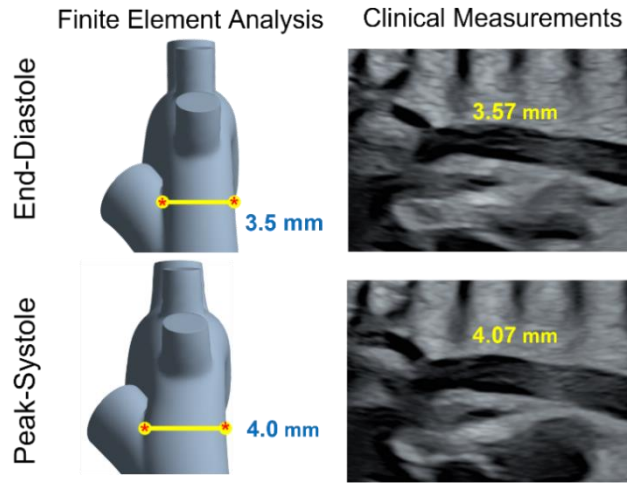


Figure 8 Comparison of vessel diameters between FEA and *in vivo* measurements for a representative subject.

Figure 8 shows the result of the estimation of material properties. Table 1 summarizes the material property and diameter changes for all subjects, showing the AoI diameters obtained in good agreement between the FEA and *in vivo* measurements.

Table 2 Material properties and vessel change of all subjects

| | Young's Modulus (MPa) | D _{AoI} in mm (min-max) | |
|-----------|-----------------------|----------------------------------|----------------|
| | | FEM | <i>in vivo</i> |
| Subject 1 | 0.15 | 1.9-2.15 | 1.9-2.18 |
| Subject 2 | 0.18 | 3.1-3.45 | 3.11-3.54 |
| Subject 3 | 0.20 | 3.1-3.5 | 3.12-3.58 |
| Subject 4 | 0.25 | 3.5-4.0 | 3.55-4.07 |

C.4 Model Verification

The proposed workflow first used the FEA to estimate the material property of the fetal aorta. Then, it estimated the Windkessel parameters for BA, LCCA, and LSA and separately adjusted the DAo parameters with FSI modeling. Therefore, it usually took a trial-and-error process to achieve all requirements, also as shown in Fig. 9:

1. In the FSI model, the total flow of the BA, LCCA, LSA, $Q_{3\text{branches}}$, reasonably matches the *in vivo* measured value, which is $Q_{AAo} + Q_{DA} - Q_{DAo}$.
2. The Q_{DAo} from FSI matches the *in vivo* measured value (error < 5%).
3. The pulse pressure of DAo (ΔP_{DAo}) from FSI matches the ΔP_{GA} (error < 5%)

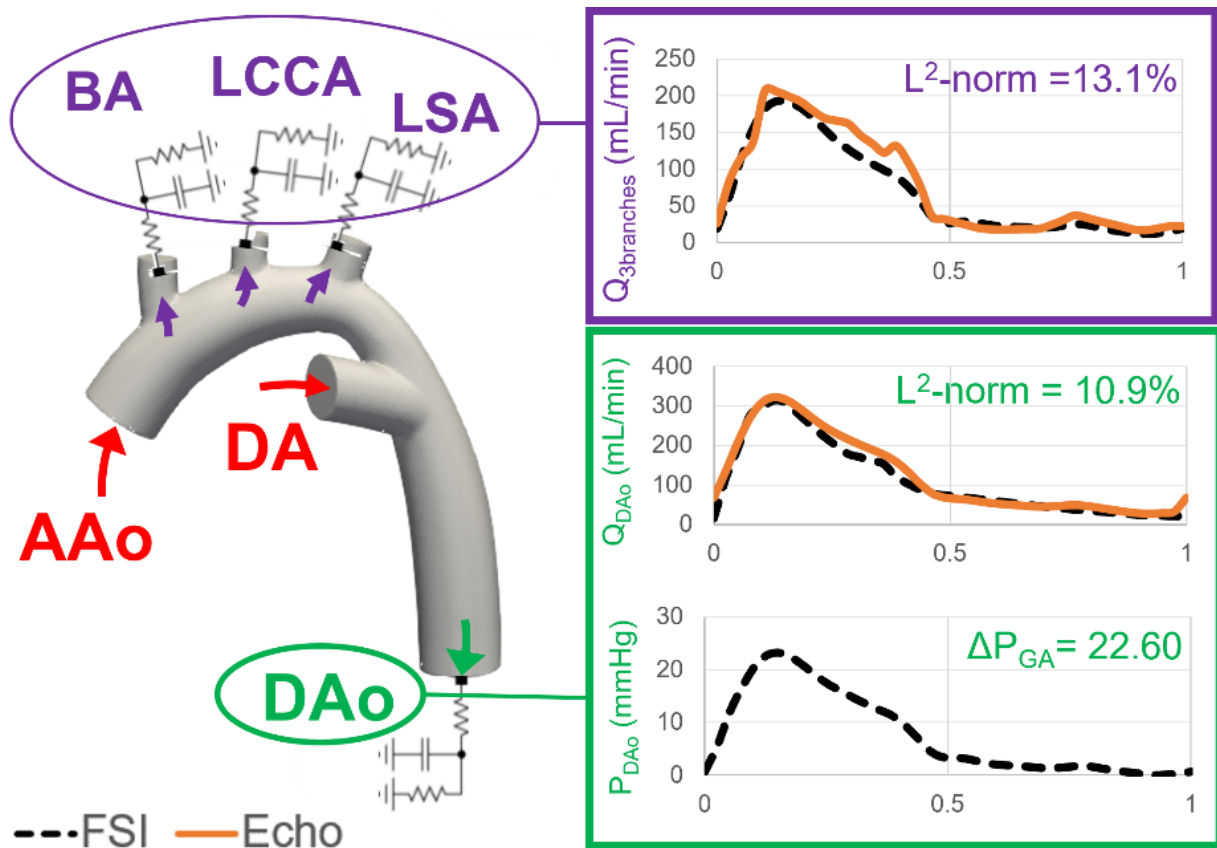


Figure 9 Model verification for a representative subject

C.5 Validation

The criteria of a successful validation were that (1) the diameter of AoI matches the *in vivo* measured value (error < 5%) and (2) the velocity at AoI reasonably agrees with the *in vivo* measurement.

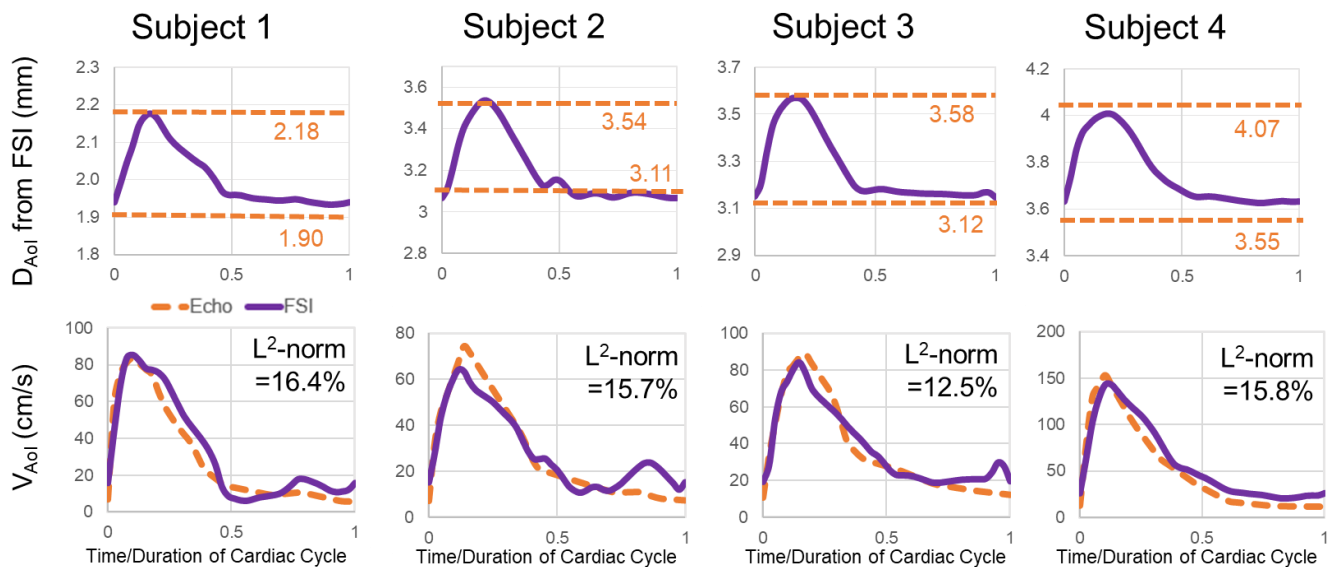


Figure 10 Comparisons for the velocity and diameter at AoI for all subjects

Figure 10 demonstrates the validation results of the proposed FSI model in four subjects. They all successfully met the two criteria.

C.6 Hemodynamics in Fetal Aorta

Figure 11 illustrates the pressure and particle tracking results for all subjects. The pressure contours explicitly depict the remarkable pressure drop from AAO to DAAo. The particle line indicates that AAO flow bifurcates into four streams: three of them flow to BA, LCCA, and LSA; the other one merges with the DA flow and exists through DAAo.

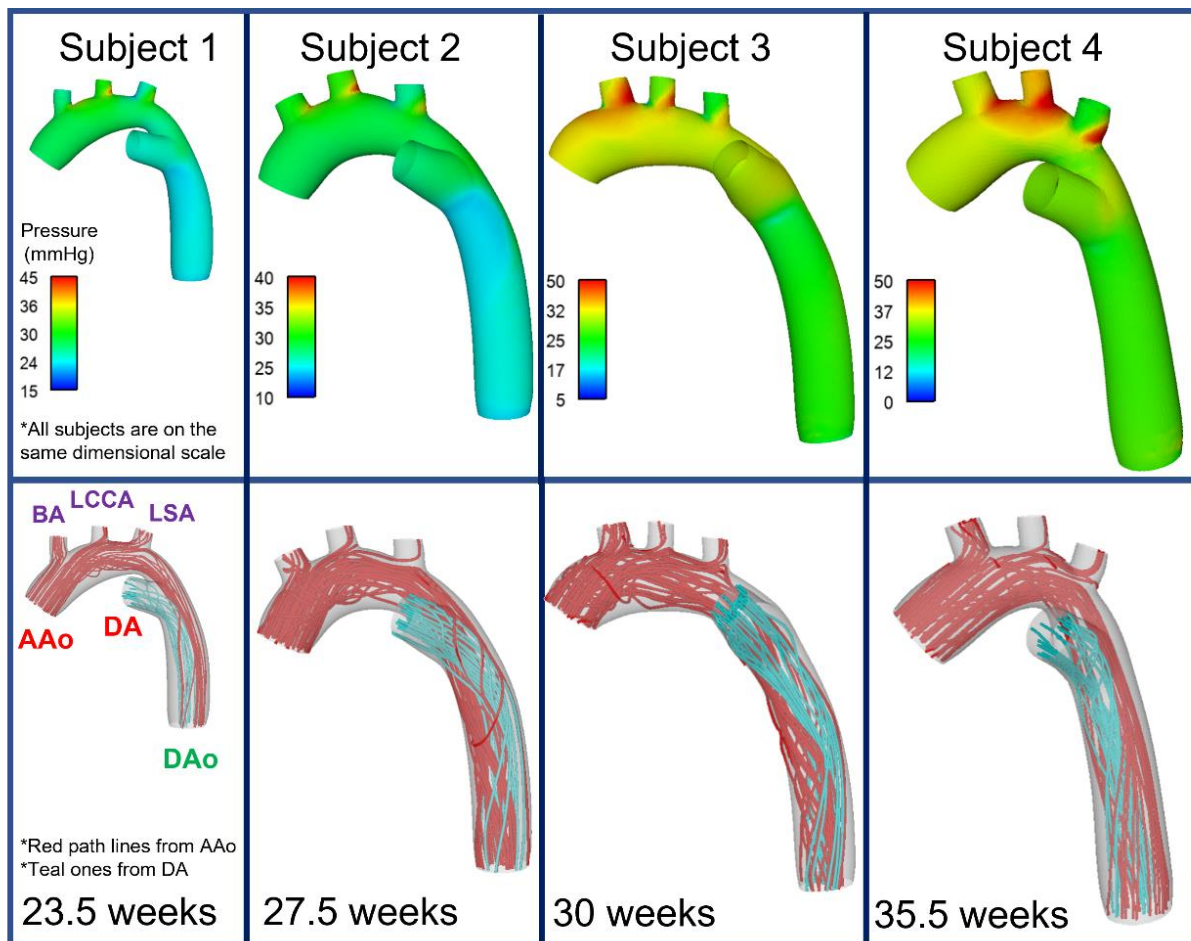


Figure 11 Pressure and particle path (colored by velocity) for all subjects

D. Discussion

D.1 Model Development and Verification

The primary difference between the fetal aorta and pediatric/adult aorta is the presence of the DA. This vessel complicates both the anatomy and FSI modeling of fetal aortas. In addition, the *in vivo*

measurement is limited, as the pressure is unavailable for all vessels. Therefore, the workflow is not trial and contains some "discontinuities", as follows:

1. It estimates the material property of the fetal aorta using FEA that achieves an agreement in DAo diameter against *in vivo* measures. However, the ultimate goal is to achieve a good agreement in FSI. Compared to a time-averaged, uniformly distributed pressure applied to the vessel in FEA, FSI has unsteady, spatially varying pressure on the vessel.
2. The estimation of the Windkessel parameters of the three branches (BA, LCCA, and LSA) was based on pulse pressure in DAo from previous literature. The primary reason is that no available data was published for these three branches or AAo. However, a remarkable pressure drop exists from AAo to DAo (as shown in Fig. 11) with the presence of the DA. This level of pressure drop does not exist in the pediatric or adult aorta.

All these "discontinuities" represent challenges for personalized FSI of the fetal aorta. It usually takes 20 trial-and-error iterations to achieve all requirements of verification. Future endeavors are warranted to explore the capability of machine learning to automate or facilitate this process.

D.2 Model Validation

The proposed flow model produced great agreements regarding vessel deformation when comparing the Aol diameter between FSI simulation and clinical measurement (Fig. 10). The in-house inverse method is a *first-of-its-kind* approach to estimating the material property of the fetal aorta. More importantly, less than 20% of the L_2 -norm was obtained in validating Aol velocity. This error level is acceptable based on previous simulation studies on fetal circulations [12, 13, 38]. Moreover, L_2 -norm is a rigorous validation metric, especially since it factors in all errors during a cardiac cycle. Previous studies validated their model concerning single velocity values, e.g., peak systole. In this study (Fig. 10), the peak velocity at Aol could achieve less than a 10% of error.

D.3 Hemodynamics in Fetal Aorta

Despite the pressure drop across the Aol, the presence of DA led to flow confluence, shown in Fig. 11. The remainder of AAo flow through Aol merges with DA flow and generates a helical flow. The

direction of flow swirling was clockwise downwards to DAo, similar to the flow within the DAo of children and adults [39, 40]. However, the helical flow observed in this study stems from flow confluence near DA in comparison to the flow within children and adults, being primarily driven by the twisting motion of heart contraction and aortic valve biomechanics. Nevertheless, the helical flow plays many positive physiological roles, including facilitating blood flow transport, enhancing nutrient transport from the blood to the arterial wall, and reducing the accumulation of atherogenic low-density lipoproteins on the endothelial surface of arteries [40].

D.4 Aortic Stiffness

Ventricular-arterial coupling, a clinically important determinant of cardiovascular performance, measures interactions between the heart and the arterial system [41-44]. Aortic stiffness is a crucial metric in the calculation of ventricular-arterial coupling. However, measuring *in vivo* aortic stiffness in fetal aortas is challenging, and previous studies adopted simplified estimations. The uncertainty of stiffness measurement resulted in conflicting trends between the aortic stiffness in fetuses and GA. Some studies demonstrated a decrease in aortic stiffness with GA [23, 32], and others reported an increasing trend [42, 43]. A few recent studies support the decreasing trend using indirect evidence. Miyashita et al. revealed a negative relationship between pulse-wave velocity and GA and suggested that pulse-wave velocity was positively correlated with vessel stiffness [44]. Zhong et al. reported a decrease in the aortic strain as GA increases, alluding that the strain was significantly negatively associated with stiffness [41]. Our inversed method was much more high-fidelity than the simplified theoretical models used in previous studies. The data reported in Table 1 supports the increasing trend of aortic stiffness with regard to GA.

E. Limitations

The present study has limitations, with the primary one being the material model. The FSI model utilized a homogenous, linear elastic material model with constant wall thickness. However, these simplifications have been widely used in previous studies for fetal and adult aorta [19, 25, 33, 34]. In addition, there is no designated validation of material properties against *ex vivo* measurement of fetal aortas. Despite the technical and ethical challenges to obtaining such measurements for healthy fetuses,

the good agreement between the obtained FSI results and clinically measured vessel size and flow velocity is technically acceptable to justify the rationale and accuracy of this approach for estimating fetal aortic material properties. Nevertheless, further investigations are warranted for more complicated material models [45, 46] and *ex vivo* validation of these models. Finally, it is worth noting that this study has a limited sample size, which is acceptable, considering most previous validations involve fewer subjects [33, 47-50].

F. Conclusions

We proposed a novel personalized flow modeling paradigm utilizing FSI, which is time-efficient and capable of simulating high-fidelity hemodynamics of the fetal aorta. This is, to date, the first paradigm that considers the personalized anatomy, flow, and material property of the fetal aorta. More importantly, this paradigm was successfully implemented and rigorously validated against clinically measured dimensions and velocities over a cardiac cycle in four fetuses representing a range of GA. Thus, this paradigm represents an important step towards developing a tool to understand the pathogenesis of CHDs related to the fetal aorta and support clinical applications such as improving diagnosis and prognosis and exploring non-invasive therapeutic strategies of these CHDs.

G. Acknowledgments

The authors acknowledge the use of ANSYS products provided through Academic Partnerships provided by ANSYS, Inc.

H. Disclosures

All authors declare that they have no conflicts of interest.

References

- [1] J.I. Hoffman, S. Kaplan, The incidence of congenital heart disease, *J Am Coll Cardiol*, 39 (2002) 1890-1900.
- [2] K. Lee, B. Khoshnood, L. Chen, S.N. Wall, W.J. Cromie, R.L. Mittendorf, Infant mortality from congenital malformations in the United States, 1970-1997, *Obstet Gynecol*, 98 (2001) 620-627.
- [3] Q. Yang, H. Chen, A. Correa, O. Devine, T.J. Mathews, M.A. Honein, Racial differences in infant mortality attributable to birth defects in the United States, 1989-2002, *Birth Defects Res A Clin Mol Teratol*, 76 (2006) 706-713.
- [4] E. Beckmann, A.S. Jassar, Coarctation repair-redo challenges in the adults: what to do?, *J Vis Surg*, 4 (2018) 76.
- [5] P. O'Brien, A.C. Marshall, Coarctation of the aorta, *Circulation*, 131 (2015) e363-365.
- [6] E.J. Dijkema, T. Leiner, H.B. Grotenhuis, Diagnosis, imaging and clinical management of aortic coarctation, *Heart*, 103 (2017) 1148-1155.
- [7] J.I.E. Hoffman, The challenge in diagnosing coarctation of the aorta, *Cardiovascular Journal of Africa*, 29 (2018) 252-255.
- [8] Z.A. Wei, M.A. Fogel, Engineering Perspective on Cardiovascular Simulations of Fontan Hemodynamics: Where Do We Stand with a Look Towards Clinical Application, *Cardiovasc Eng Technol*, 12 (2021) 618-630.
- [9] R. Mittal, J.H. Seo, V. Vedula, Y.J. Choi, H. Liu, H.H. Huang, S. Jain, L. Younes, T. Abraham, R.T. George, Computational modeling of cardiac hemodynamics: Current status and future outlook, *J Comput Phys*, 305 (2016) 1065-1082.
- [10] A.L. Marsden, Optimization in Cardiovascular Modeling, *Annu Rev Fluid Mech*, 46 (2014) 519-546.
- [11] A.L. Marsden, M. Esmaily-Moghadam, Multiscale Modeling of Cardiovascular Flows for Clinical Decision Support, *Appl Mech Rev*, 67 (2015) 1-11.
- [12] H. Wiputra, C.Q. Lai, G.L. Lim, J.J. Heng, L. Guo, S.M. Soomar, H.L. Leo, A. Biwas, C.N. Mattar, C.H. Yap, Fluid mechanics of human fetal right ventricles from image-based computational fluid dynamics using 4D clinical ultrasound scans, *Am J Physiol Heart Circ Physiol*, 311 (2016) H1498-H1508.
- [13] H. Wiputra, C.K. Chen, E. Talbi, G.L. Lim, S.M. Soomar, A. Biswas, C.N.Z. Mattar, D. Bark, H.L. Leo, C.H. Yap, Human fetal hearts with tetralogy of Fallot have altered fluid dynamics and forces, *Am J Physiol Heart Circ Physiol*, 315 (2018) H1649-H1659.
- [14] H.E. Salman, R.Y. Kamal, H.C. Yalcin, Numerical Investigation of the Fetal Left Heart Hemodynamics During Gestational Stages, *Front Physiol*, 12 (2021) 731428.
- [15] M. Malvè, M. Cilla, E. Peña, M.A. Martínez, Impact of the Fluid-Structure Interaction Modeling on the Human Vessel Hemodynamics, *Advances in Biomechanics and Tissue Regeneration 2019*, pp. 79-93.
- [16] M.N. Antonuccio, A. Mariotti, B.M. Fanni, K. Capellini, C. Capelli, E. Sauvage, S. Celi, Effects of Uncertainty of Outlet Boundary Conditions in a Patient-Specific Case of Aortic Coarctation, *Ann Biomed Eng*, 49 (2021) 3494-3507.
- [17] R. Campobasso, F. Condemi, M. Viallon, P. Croisille, S. Campisi, S. Avril, Evaluation of Peak Wall Stress in an Ascending Thoracic Aortic Aneurysm Using FSI Simulations: Effects of Aortic Stiffness and Peripheral Resistance, *Cardiovasc Eng Technol*, 9 (2018) 707-722.
- [18] V. Mendez, M. Di Giuseppe, S. Pasta, Comparison of hemodynamic and structural indices of ascending thoracic aortic aneurysm as predicted by 2-way FSI, CFD rigid wall simulation and patient-specific displacement-based FEA, *Comput Biol Med*, 100 (2018) 221-229.

- [19] M. Nowak, B. Melka, M. Rojczyk, M. Gracka, A.J. Nowak, A. Golda, W.P. Adamczyk, B. Isaac, R.A. Bialecki, Z. Ostrowski, The protocol for using elastic wall model in modeling blood flow within human artery, *European Journal of Mechanics - B/Fluids*, 77 (2019) 273-280.
- [20] P. Reymond, P. Crosetto, S. Deparis, A. Quarteroni, N. Stergiopulos, Physiological simulation of blood flow in the aorta: comparison of hemodynamic indices as predicted by 3-D FSI, 3-D rigid wall and 1-D models, *Med Eng Phys*, 35 (2013) 784-791.
- [21] A.W. Bowman, *A Practical Guide to Fetal Echocardiography: Normal and Abnormal Hearts*, 2nd ed, American Journal of Roentgenology, 195 (2010) W479-W479.
- [22] X. Zhang, H. Haneishi, H. Liu, Impact of ductus arteriosus constriction and restrictive foramen ovale on global hemodynamics for term fetuses with d-TGA, *Int J Numer Method Biomed Eng*, (2019) e3231.
- [23] P. Garcia-Canadilla, F. Crispi, M. Cruz-Lemini, B. Valenzuela-Alcaraz, P.A. Rudenick, E. Gratacos, B.H. Bijns, Understanding the Aortic Isthmus Doppler Profile and Its Changes with Gestational Age Using a Lumped Model of the Fetal Circulation, *Fetal Diagn Ther*, 41 (2017) 41-50.
- [24] P. Garcia-Canadilla, F. Crispi, M. Cruz-Lemini, S. Triunfo, A. Nadal, B. Valenzuela-Alcaraz, P.A. Rudenick, E. Gratacos, B.H. Bijns, Patient-specific estimates of vascular and placental properties in growth-restricted fetuses based on a model of the fetal circulation, *Placenta*, 36 (2015) 981-989.
- [25] P. Garcia-Canadilla, P.A. Rudenick, F. Crispi, M. Cruz-Lemini, G. Palau, O. Camara, E. Gratacos, B.H. Bijns, A computational model of the fetal circulation to quantify blood redistribution in intrauterine growth restriction, *PLoS Comput Biol*, 10 (2014) e1003667.
- [26] Z. Chen, H. Zhao, Y. Zhao, J. Han, X. Yang, A. Throckmorton, Z. Wei, S. Ge, Y. He, Retrograde flow in aortic isthmus in normal and fetal heart disease by principal component analysis and computational fluid dynamics, *Echocardiography*, 39 (2022) 166-177.
- [27] Z. Chen, H. Zhao, Y. Zhao, J. Han, C. Do-Nguyen, Z.A. Wei, Y. He, S. Ge, Diminished aortic flow in fetus and its implications in development of aortic coarctation and arch interruption: a 3D/4D fetal echocardiography and computational fluid dynamics study, *American Heart Association Scientific Sessions Virtual Meeting*, 2020.
- [28] Z. Chen, H. Zhao, Y. Zhao, C. Do-Nguyen, Z.A. Wei, a.P. Yoganathan, Y. He, S. Ge, Diminished flow in aorta by 3D/4D fetal echocardiography and computational fluid dynamics: implications in coarctation, *International Society of Ultrasound in Obstetrics & Gynecology Virtual Meeting*, 2020.
- [29] E. Tang, Z.A. Wei, M.A. Fogel, A. Veneziani, A.P. Yoganathan, Fluid-Structure Interaction Simulation of an Intra-Atrial Fontan Connection, *Biology (Basel)*, 9 (2020).
- [30] A. Updegrave, N.M. Wilson, J. Merkow, H. Lan, A.L. Marsden, S.C. Shadden, SimVascular: An Open Source Pipeline for Cardiovascular Simulation, *Ann Biomed Eng*, 45 (2017) 525-541.
- [31] M. Tree, Z.A. Wei, B. Munz, K. Maher, S. Deshpande, T. Slesnick, A. Yoganathan, A Method for In Vitro TCPC Compliance Verification, *J Biomech Eng-T Asme*, 139 (2017) 064502-064502.
- [32] P.C. Struijk, V.J. Mathews, T. Loupas, P.A. Stewart, E.B. Clark, E.A. Steegers, J.W. Wladimiroff, Blood pressure estimation in the human fetal descending aorta, *Ultrasound Obstet Gynecol*, 32 (2008) 673-681.
- [33] J. Lantz, J. Renner, M. Karlsson, Wall Shear Stress in a Subject Specific Human Aorta — Influence of Fluid-Structure Interaction, *International Journal of Applied Mechanics*, 03 (2012) 759-778.
- [34] JP van den Wijngaard, B.E. Westerhof, D.J. Faber, M.M. Ramsay, N. Westerhof, MJ van Gemert, Abnormal arterial flows by a distributed model of the fetal circulation, *Am J Physiol Regul Integr Comp Physiol*, 291 (2006) R1222-1233.
- [35] Z.A. Wei, C. Huddleston, P.M. Trusty, S. Singh-Gryzbon, M.A. Fogel, A. Veneziani, A.P. Yoganathan, Analysis of Inlet Velocity Profiles in Numerical Assessment of Fontan Hemodynamics, *Ann Biomed Eng*, 47 (2019) 2258-2270.

- [36] Z.A. Wei, P.M. Trusty, Y. Zhang, E. Tang, K.K. Whitehead, M.A. Fogel, A.P. Yoganathan, Impact of Free-Breathing Phase-Contrast MRI on Decision-Making in Fontan Surgical Planning, *J Cardiovasc Transl Res*, 13 (2020) 640-647.
- [37] Z.A. Wei, M. Tree, P.M. Trusty, W. Wu, S. Singh-Gryzbon, A. Yoganathan, The Advantages of Viscous Dissipation Rate over Simplified Power Loss as a Fontan Hemodynamic Metric, *Ann Biomed Eng*, 46 (2018) 404-416.
- [38] H.E. Salman, H.C. Yalcin, Computational Modeling of Blood Flow Hemodynamics for Biomechanical Investigation of Cardiac Development and Disease, *J Cardiovasc Dev Dis*, 8 (2021).
- [39] P.J. Kilner, G.Z. Yang, R.H. Mohiaddin, D.N. Firmin, D.B. Longmore, Helical and retrograde secondary flow patterns in the aortic arch studied by three-directional magnetic resonance velocity mapping, *Circulation*, 88 (1993) 2235-2247.
- [40] X. Liu, A. Sun, Y. Fan, X. Deng, Physiological significance of helical flow in the arterial system and its potential clinical applications, *Ann Biomed Eng*, 43 (2015) 3-15.
- [41] X. Zhong, Y. Luo, D. Zhou, M. Liu, J. Zhou, R. Xu, S. Zeng, Maturation Fetus Ascending Aorta Elastic Properties: Circumferential Strain and Longitudinal Strain by Velocity Vector Imaging, *Front Cardiovasc Med*, 9 (2022) 840494.
- [42] M. Akira, S. Yoshiyuki, Placental circulation, fetal growth, and stiffness of the abdominal aorta in newborn infants, *J Pediatr-Ur*, 148 (2006) 49-53.
- [43] M. Taketazu, M. Sugimoto, H. Saiki, H. Ishido, S. Masutani, H. Senzaki, Developmental Changes in Aortic Mechanical Properties in Normal Fetuses and Fetuses with Cardiovascular Disease, *Pediatr Neonatol*, 58 (2017) 245-250.
- [44] S. Miyashita, J. Murotsuki, J. Muromoto, K. Ozawa, N. Yaegashi, H. Hasegawa, H. Kanai, Measurement of internal diameter changes and pulse wave velocity in fetal descending aorta using the ultrasonic phased-tracking method in normal and growth-restricted fetuses, *Ultrasound Med Biol*, 41 (2015) 1311-1319.
- [45] M. Liu, L. Liang, W. Sun, Estimation of in vivo constitutive parameters of the aortic wall using a machine learning approach, *Comput Methods Appl Mech Eng*, 347 (2019) 201-217.
- [46] M. Liu, L. Liang, W. Sun, A new inverse method for estimation of in vivo mechanical properties of the aortic wall, *J Mech Behav Biomed Mater*, 72 (2017) 148-158.
- [47] W. Yang, F.P. Chan, V.M. Reddy, A.L. Marsden, J.A. Feinstein, Flow simulations and validation for the first cohort of patients undergoing the Y-graft Fontan procedure, *J Thorac Cardiovasc Sur*, 149 (2015) 247-255.
- [48] W. Mao, K. Li, W. Sun, Fluid-Structure Interaction Study of Transcatheter Aortic Valve Dynamics Using Smoothed Particle Hydrodynamics, *Cardiovasc Eng Technol*, 7 (2016) 374-388.
- [49] L. Swanson, B. Owen, A. Keshmiri, A. Deyranlou, T. Aldersley, J. Lawrenson, P. Human, R. De Decker, B. Fourie, G. Comitis, M.E. Engel, B. Keavney, L. Zuhlke, M. Ngoepe, A. Revell, A Patient-Specific CFD Pipeline Using Doppler Echocardiography for Application in Coarctation of the Aorta in a Limited Resource Clinical Context, *Front Bioeng Biotechnol*, 8 (2020) 409.
- [50] J. Sotelo, J. Urbina, I. Valverde, C. Tejos, P. Irarrazaval, M.E. Andia, S. Uribe, D.E. Hurtado, 3D Quantification of Wall Shear Stress and Oscillatory Shear Index Using a Finite-Element Method in 3D CINE PC-MRI Data of the Thoracic Aorta, *IEEE Trans Med Imaging*, 35 (2016) 1475-1487.